Available online at www.sciencedirect.com

ScienceDirect

Ceramics International 39 (2013) 9557–9566

CERAMICS INTERNATIONAL

www.elsevier.com/locate/ceramint

Doxorubicin-intercalated nano-hydroxyapatite drug-delivery system for liver cancer: An animal model

Biswanath Kundu[a,*], Debasree Ghosh[b,2], Mithlesh Kumar Sinha[a], Partha Sarathi Sen[a], Vamsi Krishna Balla[a], Nirmalendu Das[b], Debabrata Basu[a,1]

[a]*Bioceramics and Coating Division, CSIR-Central Glass and Ceramic Research Institute (CSIR-CGCRI), Kolkata 700032, India*
[b]*Drug Development, Diagnostics and Biotechnology Division, CSIR-Indian Institute of Chemical Biology (CSIR-IICB), Kolkata 700032, India*

Received 20 April 2013; accepted 16 May 2013
Available online 23 May 2013

Abstract

Hepatocellular carcinoma (HCC) is the fourth leading cause of cancer-related death worldwide, and satisfactory treatment is unavailable. Doxorubicin (DOX) is commonly used for HCC treatment with very limited success and serious side-effects such as cardiotoxicity and non-cancer cell cytotoxicity.

Methods: In the present investigation, a new nano-sized hydroxyapatite (HAp)-based drug-delivery system was successfully developed with nano-sized hydroxyapatite (HAp) (sizes 5–30 nm) and synthesised with a Ca/P molar ratio of 1.67. After thorough in vitro characterisation, these nano-HAP particles were loaded/intercalated with DOX (50–60% encapsulation efficiency), and thorough characterisation of the size, shape and morphology of the particles was performed.

Results: The average drug-loaded nanoparticles had a spherical morphology with a size range of 40–60 nm. The in vitro drug-elution kinetics were examined under different pH conditions to account for the actual pH conditions found in the body environment. The kinetics were observed to be ideal for IV therapy to treat HCC. In vivo experiments using animal models demonstrated very promising results in terms of relative liver weight changes and histopathology. Ultimately, 'high-dose' HAp-DOX produced maximum suppression of hyperplastic nodules and a minimum number of preneoplastic lesions.

In summary, our results indicate that this new formulation is an efficient, safe and reliable treatment method for HCC.

Keywords: Nano-hydroxyapatite; Hepatocellular carcinoma; Doxorubicin; In vivo; HAp-DOX conjugate

1. Introduction

Hepatocellular carcinoma (HCC) is one of the most widespread cancers worldwide. It is the fifth most common malignancy in the world and is estimated to cause half a million deaths annually. The incidence of HCC is dramatically increasing in the USA (presently it is the ninth leading cause of cancer deaths), Europe and Asia, most likely due to the increasing prevalence of hepatitis C [1,2]. HCC is a leading cause of death by cancer, and its incidence is also on the rise in developing countries [3,4]. According to Mohandas, there were approximately 14,120 patients with HCC in India in the year 2001 [5]. The mortality rates of HCC are almost the same as incidence rates.

Doxorubicin (DOX) is a drug commonly used for HCC therapy (via intra-hepatic artery delivery) but with very limited success [6–8]. DOX produces serious side-effects such as cardiotoxicity and non-cancer cell cytotoxicity. Chemotherapy of cancers is usually limited by the toxicity of drugs to normal tissues. In terms of tumour regression or overall survival, DOX has not been shown to produce clinically significant or substantial benefit [6]. Reports on multidrug resistance (MDR) arising due to the expression of the MDR gene family are also a concern [9,10]. Resection of HCC, liver

*Corresponding author. Tel.: +91 9831772081; fax: +91 33 24730957.
E-mail addresses: biswa_kundu@rediffmail.com, biswa.kundun@gmail.com (B. Kundu).
[1]Deceased 10 May 2012.
[2]Equally contributed with the First Author.

0272-8842/$ - see front matter © 2013 Elsevier Ltd and Techna Group S.r.l. All rights reserved.
http://dx.doi.org/10.1016/j.ceramint.2013.05.074

transplantation or curative excision can be achieved in a very small minority of patients, and even then, these patients still display poor survivability [11]. DOX-incorporating pegylated liposomes have been developed and display promising results in terms of long circulation times and enhanced tumour localisation in animal models [12,13]. However, the drawbacks of such treatment protocols could be outlined as follows. (1) Most of the anticancer drugs do not have specific effects on invasiveness, or they have tendency to spread throughout body. (2) These anti-proliferative drugs affect all rapidly dividing cells, including normal tissues and display dose-limiting toxic effects. (3) There is enormous drug toxicity, and numerous patient related non-compliance issues such as renal and hepatic function and bone marrow reserve. (4) The liposomal formulation of drugs may suffer from poor drug loading and self-aggregation of the drug in the entrapped state. (5) The preparative process for the nano-particles requires complex processing steps and slightly high temperature. (6) There are swelling or porosity changes with a change in pH of the polymeric formulation and some ceramic systems too, which are vulnerable to microbial attack. (7) Lastly, these polymeric formulations sometimes cannot protect the impregnated drug molecules against denaturation induced by extreme pH and temperature.

Hydroxyapatite (HAp), a hydroxylated calcium phosphate-based material, has long been known for its excellent biocompatibility, non-toxicity, non-mutagenicity, moderate resorbability with time and osteo-conductive properties [14,15]. This material has been used widely used for bone scaffolds [16], scaffold-based drug-delivery systems [17,18] and even for ocular implants [19]. Some studies have also reported HAp micro-granules/microspheres as injectable bone-filling material for intensive systemic long-term antibiotics administration [20]. However, to the best of our knowledge, nano-particulate hydroxyapatite as a carrier of doxorubicin for in vivo passive targeting of liver cancer in an animal model has not been studied. Such a study would provide and promote a long residence time in physiological fluid with reducing denaturation and toxicity of DOX. Therefore, in the present study, a nano-sized HAp-DOX system was developed, and an evaluation of its in vitro and in vivo efficacy for treating diethylnitrosamine (DEN)-induced hepatocellular carcinoma in a rat model was performed.

2. Materials and Methods

Analytical reagent-grade chemicals were used to synthesise nano-sized hydroxyapatite. Calcium nitrate tetra-hydrate [$Ca(NO_3)_2.4H_2O$] (98–100%), di-ammonium hydrogen ortho-phosphate [$(NH_4)_2HPO_4$] (99–100%), tri-ethanolamine (TEA) (98–99%), and ammonia solution (25–28%) were procured from SD Fine-Chem, India. Ultra-pure water (UPW) was used throughout all the processes and obtained using a Milli-Q system (Milli-Q Academic Century, ZMQS50001, USA).

$Ca(NO_3)_2 \cdot 4H_2O$ and $(NH_4)_2HPO_4$ were used as the source of calcium and phosphate ions, respectively. In addition, 1 M stock solutions each of $Ca(NO_3)_2 \cdot 4H_2O$ and $(NH_4)_2HPO_4$ in UPW was taken in such amounts that Ca:P molar ratio was maintained at ~1.66–1.68. The molar ratio of Ca $(NO_3)_2 \cdot 4H_2O$:TEA was varied by 1:0.01 and 1:5 and stirred for 15–45 min using a mechanical stirrer (2000–3000 rpm). The pH of the solution was maintained at 10–12 using a digital pH metre with the addition of ammonia solution. $(NH_4)_2HPO_4$ solution was added dropwise at a rate of 3–5 mL/min under vigorous stirring, keeping the pH of the solution at 9–11. The gelatinous precipitate thus obtained was filtered and washed thoroughly by UPW using a centrifuge. The precipitate was dried in a freeze drier (Eyela, FDU-2200, Japan) at −80 to −85 °C (at 10–20 Pa).

DOX-conjugation experiments were conducted independently in UPW. Doxorubicin hydrochloride (≥98%) was procured from Aldrich, USA. It was first dissolved in UPW by rapid mixing in a vortex apparatus for 5–10 min just prior to their use in the adsorption studies. The DOX concentration was varied between 5 and 20 μg/mL.

Samples of hydroxyapatite nano-powders (3–7 mg) were dispersed in 2–4 mL of DOX solution in a 15-mL capacity conical poly-ethylene tubes by rapid mixing in a Vortex apparatus (Eppendorf MixMate PC 13-08, Germany) for 1–2 min at 2500–3000 rpm. Thereafter, three steps were followed for the above conjugation: (i) mechanical agitation (GL 83, Toshniwal Flask shaker, India) and ultrasonication (Electronic Industries, India) (at 1.5–2.5 kW for 30–45 min), (ii) vortex mixing (at 3000 rpm for 30–45 min) again at high vacuum (0.01–0.001 Torr) and finally, (iii) high-speed refrigerated centrifugation (Heal Force, Neofuge 23R, China) at 15,000–18,000 rpm (at 8–10 °C for 15–30 min) with a normal pH range (7–8). The supernatant was collected for the estimation of DOX concentration to obtain the uptake of DOX by the nano-HAp. The uptake of DOX by the slurry of hydroxyapatite was determined from the relation: $Q = V(\Delta C)/W$, where Q (mg/g) is the amount of DOX sorption, V (L) the volume of the solution in contact with W (g) of HAp, and ΔC (mg/L) the difference between the initial (C_0) and final (C_e) equilibration concentrations. The values of the sorption of DOX by the hydroxyapatite were reproducible within a range of ~5% (after two or three trials). The values of C_0 and C_e were obtained with a UV Vis Spectrophotometer (Lambda 45, Perkin-Elmer, USA), and the absorbance value of DOX at the 481-nm wavelength. Molar absorptivity (ε) values were obtained using Beer-Lambert's equation [$\varepsilon = A/(cl)$], where A is the absorbance, c is the sample concentration in mol/L, l is the length of light path through the sample in cm (length of the cuvette, i.e., 1 cm) and ε has the unit of L mol^{-1} cm^{-1}. From the ε values, the concentration of supernatant was calculated. All C_0 and C_e values were obtained after obtaining the calibration curve of DOX using different concentration of DOX, e.g., 0.025–5 μg/mL. The DOX adsorption was expressed as mg of DOX adsorbed per g of HAp nano-particles. The precipitate was washed thoroughly with UPW to remove the free DOX by repeated centrifuging (for at least five times) at 5000–8000 rpm at 8–10 °C for 15–20 min and subsequently freeze dried at –80 to 85 °C (at 10–20 Pa) for 24–48 h to obtain the drug-loaded powders. Both the bare nano-particles and

DOX-loaded samples were characterised by X-ray diffraction (XRD, Philips Analytical B.V., X'Pert Pro, The Netherlands), Fourier-transformed infrared spectroscopy (FTIR, Perkin-Elmer, Spectrum 100, USA), field emission scanning electron microscopy (FESEM, Supra 35 VP, Carl Zeiss, Germany) and transmission electron microscopy (TEM, Tecnai G2 30, FEI, The Netherlands) to determine the different parameters previously mentioned were performed. The XRD was performed using a powder diffractometer. The continuous data were collected over a 2θ range 20–60°, using monochromatic Cu $K_{\alpha 1}$ radiation (operating conditions being 30 mA and 40 kV and wavelength of 1.5406 Å), with a step size of 0.017° and a count time of 10.34 s. The diffraction patterns were compared with the JCPDS PDFs (Joint Committee on Powder Diffraction Standards Powder Diffraction Files) database. For the FTIR, the alkali halide disk technique was employed using ~2 mg of respective powders in 200 mg of powdered spectroscopic grade KBr (FTIR grade, Merck KGaA, Germany) that had been dried at 100 °C and allowed to cool in a vacuum desiccator to avoid absorption of moisture. The middle-IR spectra (4000–400 cm^{-1}) were obtained using the aforementioned instrument, which was purged of H_2O-vapour and CO_2 with an air drier. The absorption bands of H_2O vapour, CO_2 and polystyrene film were used to calibrate the spectra in this region. The wavenumber accuracy of all sharp bands was $\pm 2\ cm^{-1}$. For the FESEM, the powder particles were suspended in ethanol, mechanically shaken for 30 min, immersed in an ultrasonic bath for another 30 min and finally the supernatant was collected, and a few drops of the same was spread on a watch glass before observation. The dried powder was then sputter-coated (Polaron, Quoram Technology, U. K.) with gold-palladium having a coating thickness of ~6 nm to reduce charging and to improve the image quality prior testing. The samples for TEM observation were prepared by dispersing some products in ethanol and immersing them in an ultrasonic bath for 30 min, and a few drops of the resulting suspension were placed onto a copper grid (300 mesh) coated with a layer of amorphous carbon on filter paper and dried in air. TEM was performed at an accelerating voltage of 300 kV. Finally, TGA (thermogravimetric analysis) was performed (STA 409, Netzsch GmbH, Selb, Germany) using an exact quantity of particles subjected to heat treatment up to 1000 °C (with a heating rate of 10 °C/min), and the weight losses were recorded to calculate the adsorption efficiency.

The desorption of the DOX from hydroxyapatite was conducted in contact with three different buffers having different pH conditions (1.2, 4.9 and 7.4) at a temperature of 37.4 °C for a time period of 0–24 h. To obtain pH 7.4 buffer, the following composition was used: 8 g of NaCl, 0.2 g of KCl, 1.15 g of Na_2HPO_4, 0.2 g of KH_2PO_4 in 1 L of UPW. For pH 1.2 buffer, 50 mL of 0.2 M KCl, 85 mL of 0.2 M HCl and water were used to make 200 mL of this buffer. For pH 4.9 buffer, 40 g of NaH_2PO_4, 1.2 g of NaOH and water was used to make 100 mL of buffer. These pH conditions were selected to mimic the actual pH conditions encountered whenever any foreign particles enter into the body physiological fluid system. In addition, 3–4 mg of HAp-DOX particles were added to 3 mL of each of the above buffers and were kept for 0 h, 1 h, 2 h, 4 h, 8 h, 12 h and 24 h at a temperature of 37.4 °C. After each interval, 1.5 mL of supernatant was collected with replenishment of the same amount of fresh buffer. These samples were analysed with a UV Vis Spectrophotometer to determine concentration as previously described. As before, the calibration curve for the DOX was created using 0.025–5 μg/mL of DOX solution prior the concentration estimation. The sample collection was conducted without shaking the vials.

In the in vivo experimentation, adult female Swiss Albino rats (with an average weight of 100–120 g) were adapted to the laboratory environment for 7 days (26–28 °C, 60–80% relative humidity, 12 h light/dark cycle) before starting the treatment. The rats were supplied with food and drinking water ad libitum. The rats were divided into five groups, and each group contained 5 animals. The rats in the normal group were injected with three intraperitoneal (IP) injections of olive oil in 15-day intervals. The rats in the DEN-administered groups were given three IP injections of DEN (200 mg/kg of body weight) in 15-day intervals. These rats served as the control group. Free DOX (1 mg/kg of body weight) was injected into the tail veins of the DEN-administered group of rats (1 week after the last IP injection of DEN), once a week for four weeks. HAp nano-particles without DOX (equivalent to 1 mg/kg of body weight) were injected into the tail veins of rats in the other DEN-treated group (1 week after last IP injection of DEN), once a week for 4 weeks. The final formulation of HAp-DOX was injected into the tail vein of the last DEN-injected group of rats (1 week after last IP injection of DEN), once a week for 4 weeks. One week after the experiment, the rats were sacrificed by cervical dislocation. All the rats used in this study received proper care and handling in compliance with the Animal Ethics Committee, India (Registration no. 147/99/CPCSEA, India). The livers were immediately fixed in 10% formalin and processed for histological examination. Liver histology was studied by microscopic examination of haematoxylin-eosin stained sections.

3. Results and discussion

X-ray diffraction of the as-synthesised powder (Fig. 1a) indicated that the power was composed of hydroxyapatite, which matched with the JCPDS PDF no. 74-0566 published by ICDD (International Centre for Diffraction Data). The relative positions of the major peaks matched with the standard [e.g., (211) I_{100} peak at 31.766° 2θ, (112) I_{52} peak at 32.195° θ and (300) I_{63} peak at 32.897°2θ]. The average crystallite size (D) calculated by Scherer's equation (FWHM: full width at half maxima) was calculated and determined to be ~8.13 ± 3 nm. The following equation was used for the purpose with (002) I_{29} peak at 25.883° 2θ:

$D = (0.9\lambda/(\beta\cos\theta))$, where λ is the wavelength of the monochromatic x-rays used (0.54056 nm), β is the broadening of diffraction peak at half of its maximum intensity in radians and θ is the diffraction angle (25.883° in this case). The estimated particle sizes were compared with the FESEM or TEM

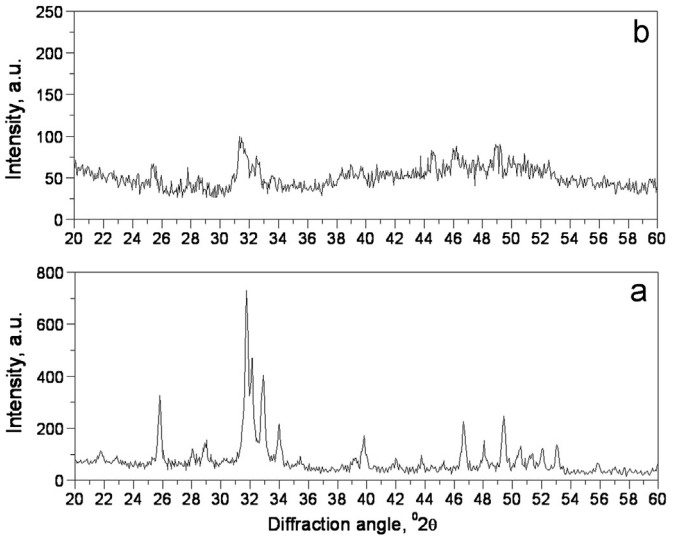

Fig. 1. XRD plot of (a) bare nano-hydroxyapatite particles and (b) conjugated formulation of HAp-DOX.

microstructure of the same powders (Fig. 3a and b). It was observed that the primary particle (or crystal) sizes estimated using Scherer's equation correlated very well with the microstructural study results. Cauliflower-like microstructures were obtained, which after thorough and prolonged dispersion by ultrasonication, displayed nicely dispersed HAp particles with a size ranging between 15 and 50 nm and having more-or-less hexagonal geometry. TEA was used to periodically restrict the nuclear growth of the reaction between calcium nitrate and di-ammonium hydrogen ortho-phosphate. TEA has a tetradentate molecular structure with the same bonding mode with other molecules. TEA does not have any tendency to solubilise Ca^{2+} ions, and it restricted the nuclear growth of HAp nano-particles while the reaction was continuing between the other reactants. These results corroborated the findings of Pramanik et al. [21]. When the powder was used to entrap the DOX, the XRD pattern (Fig. 1b) of the conjugated particle indicated DOX adsorption on the nano-HAp surface, which resulted in reduction of peak intensities of crystalline peaks of HAp as observed in as-prepared bare nano-particles (Fig. 1a). The amorphous nature of the pattern was also increased (Fig. 1b) mainly due to the organic moiety covered on the HAp surface. Similar observations were made by Yu and Chow for their nano-conjugation system [22]. We have designated two formulations of HAp-DOX according to the HAp surface adsorption, detailed below, as 'low dose' and 'high dose'. From the microstructures of the DOX-loaded HAp surface (Fig. 3c and d) of both the 'low-dose' and 'high-dose' formulations, it was observed that DOX was attached to the HAp nano-particles and became spherical upon DOX-loading most likely because of the high surface tension of the DOX solution on the HAp surface facilitated by the highly negative surface charge of HAp [18]. The average particle size for the 'low-dose' and 'high-dose' formulations was determined to be ~25 nm and 32 nm, respectively. It should be mentioned here that these two doses were calculated from the equations mentioned above using absorbance values of UV Vis spectrum at 481 nm. After high-speed centrifugation at 15,000–18000 rpm, the supernatant DOX concentration values were used to calculate the DOX absorption/adsorption of HAp surface. These were observed to be 25 ± 5 mg/g of nano-HAp particles for the 'low-dose' formulation and 95 ± 5 mg/g of nano-HAp particles for the 'high-dose' formulation. We also examined the interface microstructure of DOX and the nano-HAp particles by TEM to understand the nature of DOX adsorption. These images are provided in Fig. 4a and b. It was observed that DOX was adsorbed on the surface without any intercalation inside the HAp crystal. The thickness of the DOX coating on average was observed to be ~3.9 nm and 8.7 nm for the 'low-dose' and 'high-dose' formulations, respectively. The crystal planes of HAp and the DOX coating on its surface could be clearly seen as shown in Fig. 4a and b. There was no interfacial gap between these two, which suggests that either the DOX was reacted on the surface of Hap, which lead to chemical covalent bonding, or it was simply adsorbed on the HAp surface by some type of ionic/secondary bonding (e.g., hydrogen/OH^- bonding). These results were correlated with the FTIR spectrum results, which will be discussed later. TGA was used to calculate the encapsulation efficiency [23]. The exact quantity of bare nano-particles, DOX and drug-loaded HAp (both the 'low' and 'high' dose formulations) were used for the calculation. It was observed that, on average, the drug (DOX) encapsulation efficiency of HAp nano particles were ~30% and ~52% for the 'low-dose' and 'high-dose' formulations, respectively.

The basic structure of the DOX molecule (shown in Fig. 5) contains four cyclic groups, which makes this molecule interactive with DNA base pairs [24]. The chemical reaction between the DOX and the DNA base pairs results in DNA intercalation, which leads to the halting of DNA replication and thus the death of tumour cells [25]. DOX is a tetracyclic molecule, containing three planar and aromatic hydroxyanthraquinone rings, which function as a chromophore, and one nonplanar, nonaromatic ring attached to an aminoglycosidic side chain. As the DOX molecule contains various functional groups (–C═O, –COOROH, –OH, –OR, $–NH_3$, etc.) within the DOX molecule, as a result it can easily interconvert from one functional group to other (e.g., enol to keto) by changing the pH of the solution. Ultraviolet absorption shows the maximum absorption peaks centred at 233, 250 and approximately at 481 nm. Fig. 2 represents the FTIR spectra of (a) bare nano-hydroxyapatite particles, (b) free doxorubicin, (c) conjugated formulation of HAp-DOX ('low-dose') and (d) conjugated formulation of HAp-DOX ('high dose'). The following few assignments of bands of DOX (Fig. 2b) were as follows for different wavenumbers:

3436h: ν HO–H;
2929w: ν $C^{33/35/37}$–H;
2851vw: ν $C^{33/35}$–H;
1730h: δ N–H;
1619h: ν Ring, δ CO^{25}–H;
1585h: Ring breathing, Ring (Phe), δ C–H (aro);

1414h: Ring, Ring–O, δ N–H, Ring$=$O, δ $C^{13/31/33/37}$–H, δ C^{32}–H_2 Ring, δ C^{35}–H_3;
1377h: δ C^{13}–H, δ O–H$\cdots$O, δ C–C, C^{16}–OH;
1286h: δ O–H$\cdots$O, δ C^{11}–OH, C^{13}–H;

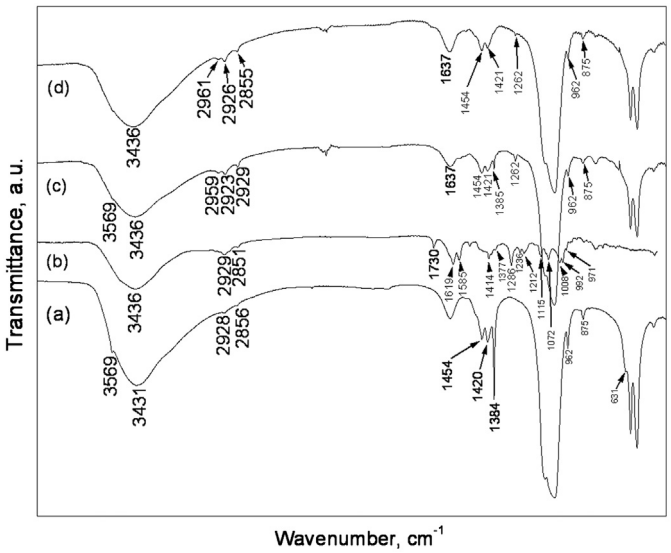

Fig. 2. FTIR spectra of (a) bare nano-hydroxyapatite particles, (b) free doxorubicin, (c) conjugated formulation of HAp-DOX ('low dose') and (d) conjugated formulation of HAp-DOX ('high dose').

1236m: Ring, $C^{22/15}$–H_2, CO–H;
1115m: Ring, C–H (aro), C^{30}–H;
1072m: δ C^{16}–C^{15}–H, C^4–O^6–C^{30}, δ N–H_2, δ C–H_x (ali);
1008h: ν C^{13}–O^{14}–C^{31}, ν C^{16}–O^{17}H, δ C–H_x (ali); and
992h: δ C–C$=$O, C–OH, δC–H_x (ali),

where, w, vw, m, h, Phe, aro, ali represent weak, very weak, medium, high band intensity, phenyl, aromatic and aliphatic groups, respectively, and ν and δ denote stretching and bending vibrations, respectively.

On the other hand, the band assignments for the bare HAp nano-particles are given as follows:

3700–3000: H–O–H, Water of crystallisation or adsorbed water;
3580: O–H, (OH) group;
1615: H–O–H, Water of crystallisation or adsorbed water;
1454, 1414: C–O of CO_3 groups;
1119, 1098: P–O and P–OH, HPO_4, and PO_4 groups;
1030: P–O in HPO_4, and PO_4 groups (stretching mode);
965: P–O in PO_4 group;
865: P–OH stretching mode of HPO_4 groups;
630: O–H of OH group;
600, 564: P–O in PO_4 groups (bending mode); and
525: HO–PO_3 bending mode in HPO_4.

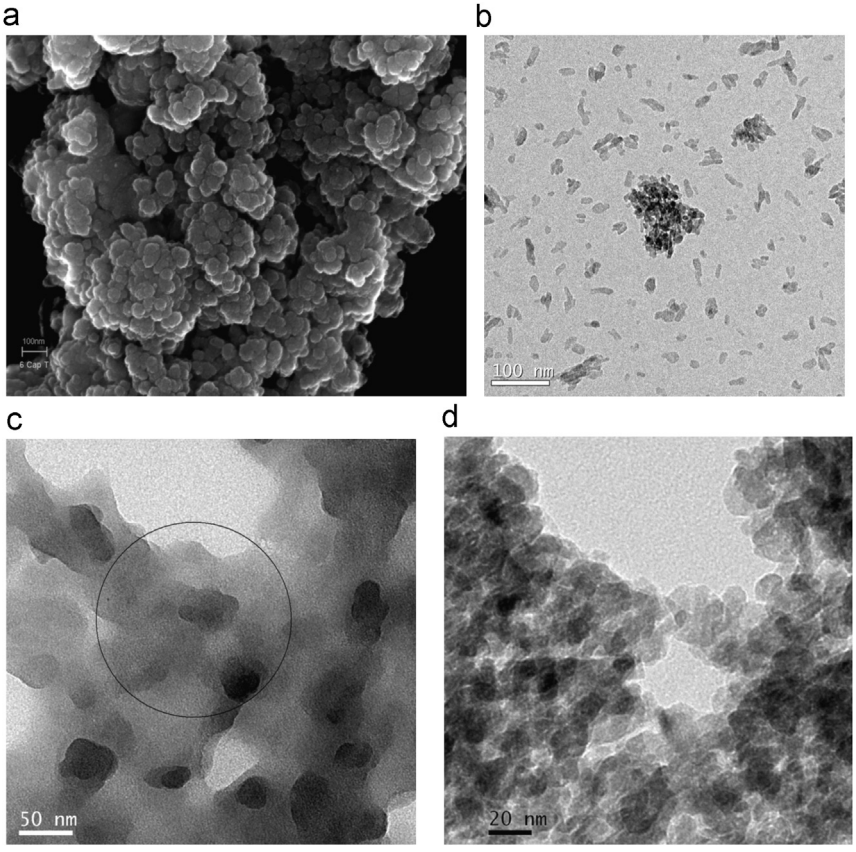

Fig. 3. (a) FESEM morphology of bare nano-hydroxyapatite particles, (b) bare nano hydroxyapatite highly dispersed and observed under TEM, (c) conjugated formulation of HAp-DOX ('low dose') and (d) conjugated formulation of HAp-DOX ('high dose') observed under TEM.

It was evident that the respective functional groups for PO_4^{3-} and OH^- corresponding to HAp crystals were present in Fig. 2a. A very small peak at the wave number 1454 cm^{-1} in this figure arose from vibrations of CO_3^{2-} ions. Bands at 3431 and 1615 cm^{-1} arose from adsorbed molecular water. The bands at 1454 and 1420 cm^{-1} attributed to CO_3^{2-} groups in the apatite structure are well defined [26]. In Fig. 2a, the carbonate band at 1454 cm^{-1} corresponds to the incorporation of CO_3^{2-} groups at the OH^- position (A-type) and the same band at 1420 cm^{-1} corresponds to the occupation of PO_4^{3-} sites in the apatite structure (B-type). The band at 875 cm^{-1} was assigned to both types of incorporation [27,28]. It may be concluded that some carbonates were incorporated during the synthesis of nano-Hap that had a synergistic role for subsequent DOX attachment. The band at 1384 cm^{-1} could be due to the presence of $–CH_2–$. These functional groups of nano-HAp can interact with different molecular groups of DOX, particularly the amino and several hydroxyl groups (Fig. 5). The –OH and carbonate groups on the HAp crystal can form a strong hydrogen-bonding interaction with the –OH and $–NH_2$ groups in DOX. The absence of an OH^- group (which is the characteristic of HAp crystal) in Fig. 2c and d could be due to the secondary bonding OH···H (weak hydrogen/Van der Waal's bonding) formation of the nano-hybrid between DOX and HAp. There were some shifting of peak positions of DOX at 2929 and 2851 cm^{-1} to lower positions when the adsorption of DOX occurred on the surface of HAp, which was indicative of formation of hydrogen bonding between C–H (of DOX) and HAp. Some other observations include the following:

(1) The absence of peak at 1730 cm^{-1} in DOX when incorporated in HAp (Fig. 2c and d); this peak shifted to a lower wavenumber, and there was peak broadening at 1637 cm^{-1}, indicative of the interaction of the HAp crystal on the δ N–H part of the DOX.
(2) The reduction of the transmittance of 1384 cm^{-1} peak of bare nano-HAp (Fig. 2a) in contact with DOX and the subsequent absence of this peak when the DOX loading was increased ('high-dose'). This was indicative of secondary bonding between δ O–H···O (of DOX) and $–CH_2–$ of HAp.
(3) There was, as such, no significant interaction between the phosphate groups of HAp with any other functional groups present in DOX.

To design a controlled drug-delivery system, it is important to consider changes of pH at specific or physiological sites in the body (e.g., changes of pH in gastrointestinal tract, bacterial enzymes localised within the colon, etc.) [29]. A specific drug can be released at a target site when there is a difference in pH. Cancerous or infected tissue pH is higher than that of normal tissue [30]. In the present investigation, before obtaining the

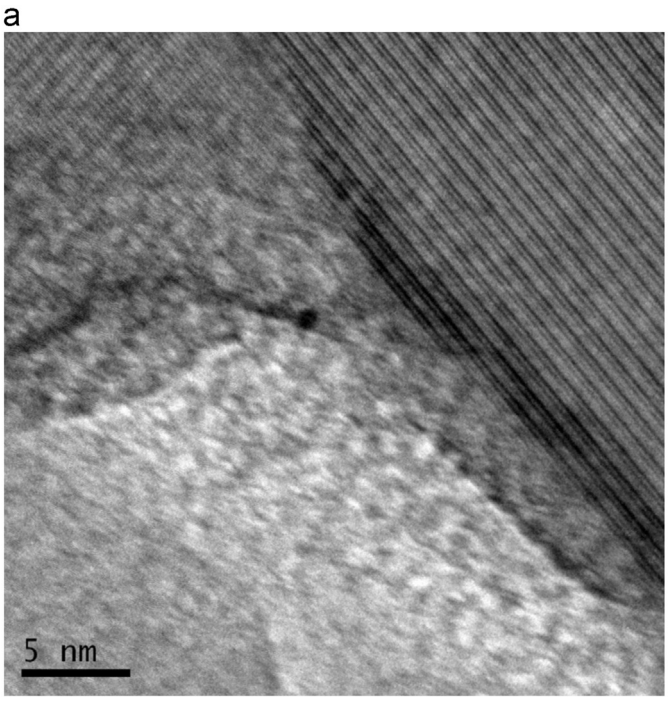

Fig. 4. High-resolution TEM morphology of conjugated formulation of HAp-DOX; (a) 'low dose' and (b) 'high dose'.

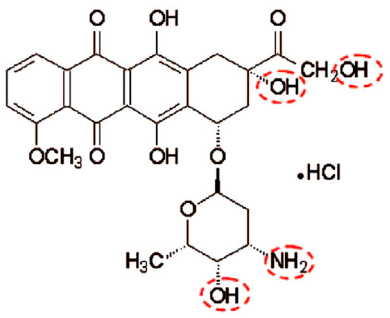

Fig. 5. Basic molecular structure of doxorubicin.

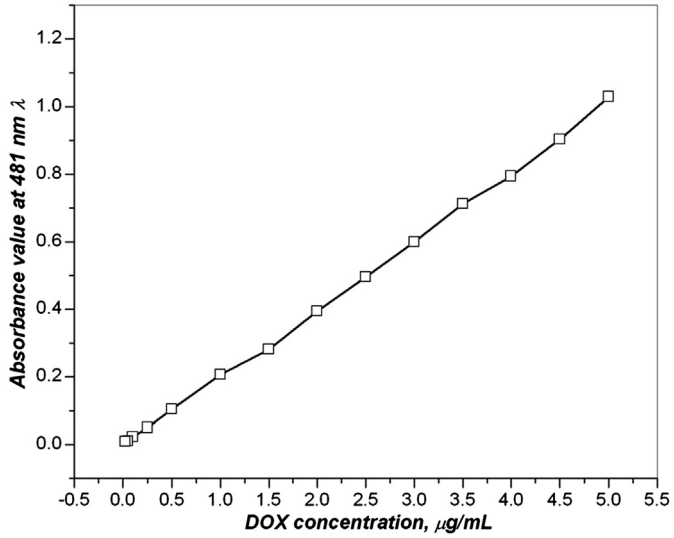

Fig. 6. Calibration curve obtained from the 481-nm absorbance values of the UV Vis spectra at different concentration of DOX aqueous solution. This curve was subsequently used for the determination of the elution kinetics of DOX at different pH conditions at 37.4 °C.

elution kinetics under different pH conditions at 37.4 °C, different concentrations of DOX were evaluated for linearity, or a calibration curve was obtained with the absorbance values at 481 nm of UV Vis spectra w.r.t. the actual concentration of DOX aqueous solution. This curve is given in Fig. 6. From this curve, the elution profiles at different pH conditions were plotted and are given in Fig. 7a–c. It was observed that irrespective of the pH conditions, the elution rate of DOX was lower for 'high-dose' samples and continued even after 13 h. At low pH, 'low-dose' samples continue to elute up to 13 h and at pH 7.4, and the drug release was almost complete at 13 h. The drug release rate was faster for the 'low-dose' samples than the 'high-dose' samples at all pH studied. These three pH values were selected because of the possible encounter of HAp-DOX nano-particles at different physiological pH conditions while traversing through blood and finally absorption into the liver cancer cells. Due to the lower adsorption of DOX in 'low-dose' samples, drug elution was much faster due to the partial dissociation of hydrogen bonding interaction under higher acidic conditions as well as at pH 7.4. The formulation was thus optimised w.r.t. these properties. The

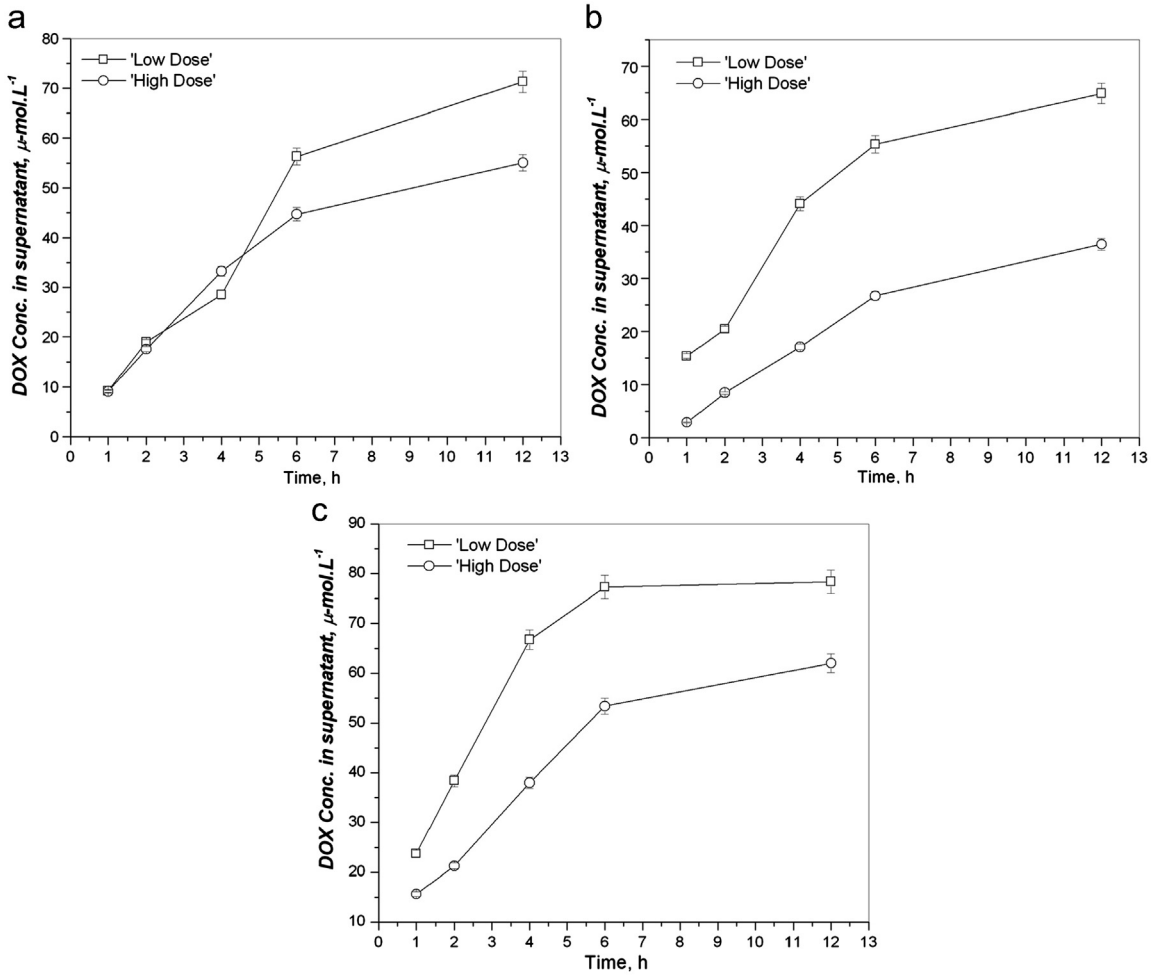

Fig. 7. DOX elution profile with time for conjugated formulation of HAp-DOX in contact with different buffers maintained at (a) pH 1.2, (b) pH 4.9 and (c) 7.4.

Table 1
Effect of DOX (free and in HAp conjugated forms) on % increase in relative liver weight (RLW) in DEN induced hepatocarcinogenic rats, where the results are expressed as mean ± S.E. of five rats.

Experimental groups	No. of rats	Final body weight (g)	Liver weight (g)	RLW	% increase of RLW
Normal	5	196 ± 3.2	8.2 ± 0.2	4.2 ± 0.14	–
DEN treated (A)	5	152 ± 2	10.5 ± 0.16	6.9 ± 0.21*	64.2
(A)+Free DOX treated	5	155 ± 3.3	10.1 ± 0.18	6.5 ± 0.27	54.7
(A)+Bare HAp nano particle treated	5	155 ± 2.7	10.0 ± 0.16	6.5 ± 0.23	54.7
(A)+'High dose' HAp-DOX treated	5	192 ± 1.4	8.6 ± 0.11	4.5 ± 0.1**	7.1

*Indicates significant difference from normal ($P < 0.0001$).
**Indicates significant difference from the DEN administered group (A) ($P < 0.0001$).

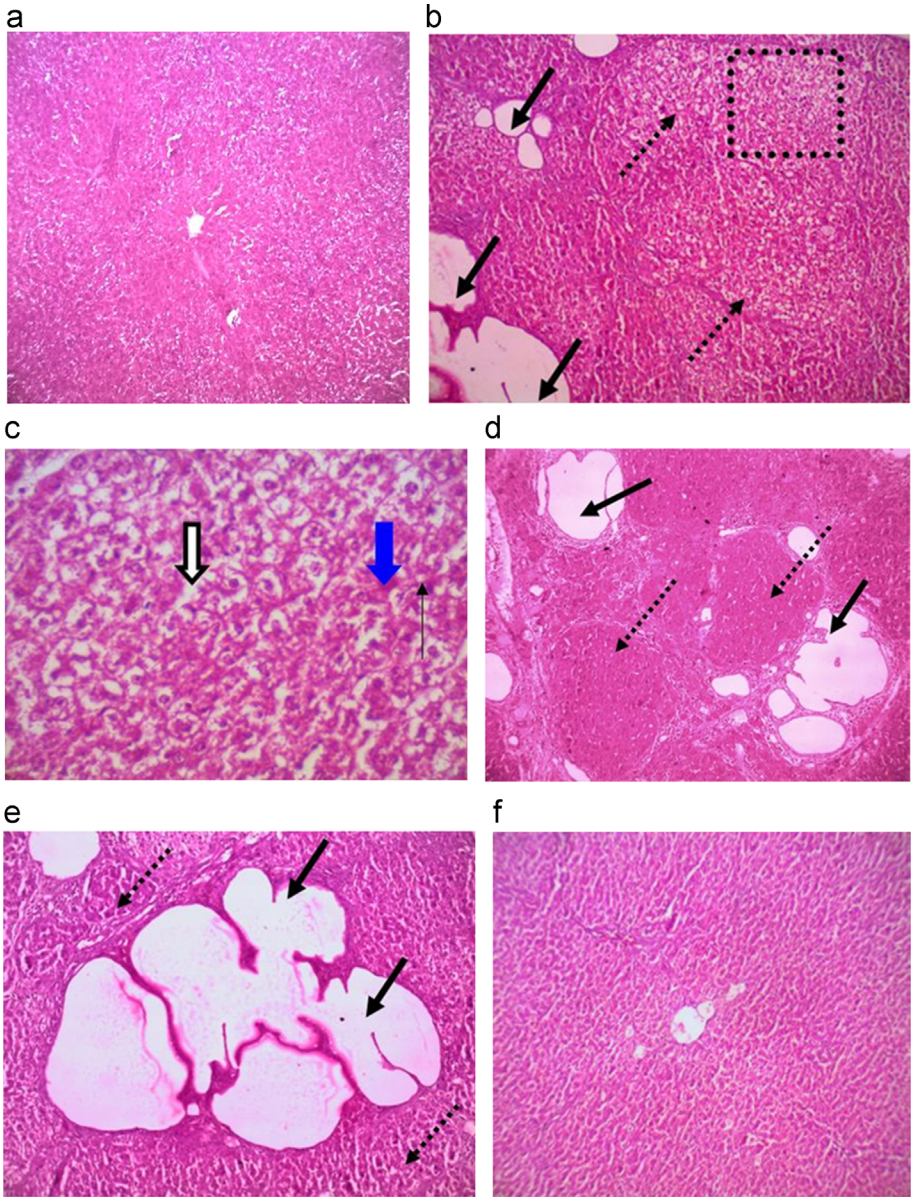

Fig. 8. Histopathological images of haematoxylin-eosin stained liver sections. (a) Normal (× 100), (b) DEN treated [A] (× 100), (c) DEN treated [A] (× 400), (d) [A]+free doxorubicin treated (× 100), (e) [A]+empty nano HAp treated (x 100) and (f) [A]+nano HAp-doxorubicin treated (× 100). The solid thick black arrows indicates a dialated hepatic vein, the broken black arrow indicates hepatic micronodules, the hollow black arrow indicates fatty changes, solid thick blue arrow indicates eosinophilic cytoplasm and the thin black arrow indicates an atypic nucleus. (For interpretation of the references to colour in this figure legend, the reader is referred to the web version of this article.)

'high-dose' formulation displayed high elution under acidic conditions (pH 1.2), which can be ideal for cancer cell delivery of DOX. Finally, due to its high entrapment efficiency, along with its superior and prolonged in vitro elution kinetics, the 'high-dose' HAp-DOX was used in the in vivo experiments to combat DEN-induced hepato-cellular carcinoma (HCC) in a rat model. This drug-delivery formulation and system (intravenously applied) was developed to optimise the therapeutic properties of the anti-cancer drug DOX for safety, effectiveness and reliability. The DEN-induced rat liver cancer model has been previously described by Ghosh et al. [31].

The pathological liver conditions can be evaluated by increases in relative liver weight as compared with a normal liver. DEN (3 doses of IP 200 mg/kg of body weight at 15-day intervals) administration causes an increase in the relative liver weight (RLW) in rats. Free DOX or bare HAp nano-particles proved almost ineffective against hepatocellular carcinoma. 'High-dose' HAp-DOX nanoparticles reduced RLW significantly in comparison with the DEN-administered control group (Table 1). A reduction of RLW of rats following treatment with 'high-dose' HAp-DOX nanoparticles is an important indication of improvement in the pathological liver condition.

The hepatocarcinoma in rats were evaluated via histopathological examination. Haematoxylin-eosin-stained liver sections of normal rats (Fig. 8a) showed that hepatocytes are arranged in cords around hepatic veins, forming hepatic lobules. Portal tracts were observed to be are normal. The DEN-injected animals displayed dilated hepatic veins and hepatic micronodules separated by thin fibrous septum (Fig. 8b). At higher magnification, the fatty changes in hepatocytes with some eosinophilic cytoplasm and atypic nucleus are evident (Fig. 8c). All these features observed in DEN-injected control group of rats are very important markers of hepatocellular carcinoma [32]. There were no significant changes to the DEN-induced hepatocyte pathomorphological structures with free drug treatment. The hepatic micronodules separated by thin fibrous septa with dialated hepatic veins are evident (Fig. 8d). Bare HAp nano-particles were also not effective in combating DEN-induced hepatocellular carcinoma (Fig. 8e). However 'high-dose' HAp-DOX was extremely effective in combating hepatocellular carcinoma. Normal-looking hepatic veins, portal tracts and hepatocytes were present following treatment with 'high-dose' HAp-DOX (Fig. 8f).

4. Conclusion

Nano-sized hydroxyapatite with an average crystallite size ~8.13 ± 3 nm and cauliflower-like nano-particles with a size range between 15 and 50 nm that have more-or-less hexagonal geometry were synthesised in the laboratory. The synthesised HAp powder with an average particle size of ~25 nm and 32 nm was encapsulated with the drug DOX to obtain a concentration of two formulations that were termed as 'low' and 'high' dose depending on DOX adsorption on nano-HAp particles (25 ± 5 mg/g cf. and 95 ± 5 mg/g), respectively, and with an encapsulation efficiency of ~30% cf. ~52% with an average particle size of ~25 nm and 32 nm, respectively. The thickness of DOX coating on the HAp was observed to be ~3.9 nm and 8.7 nm, respectively. The –OH and carbonate groups on the HAp crystal can form a strong hydrogen-bonding interaction with –OH and $–NH_2$ groups in DOX. The drug-elution kinetics in different pH conditions indicated that irrespective of pH conditions, the elution rate of DOX with time was lower for the 'high-dose' samples, and the elution continued even after 13 h. Due to the lower adsorption of DOX in the 'low-dose' samples, drug elution was much faster due to partial dissociation of the hydrogen bonding interaction under higher acidic conditions as well as at pH 7.4. The 'high-dose' formulation displayed higher elution of DOX under acidic conditions (pH 1.2) after 6 h, which can be ideal for cancer cell delivery of DOX. Finally, due to its high entrapment efficiency, along with its superior and prolonged in vitro elution kinetics, the 'high-dose' HAp-DOX was used under in vivo conditions to combat diethylnitrosamine (DEN)-induced hepato-cellular carcinoma (HCC) in a rat model. This drug-delivery formulation and system (intravenously applied) was developed to optimise the therapeutic properties of the anti-cancer drug DOX for safety, effectiveness and reliability.

Acknowledgements

The authors wish to express their sincere thanks for the financial support of the Council of Scientific and Industrial Research, India (41/3/EFYP/IAP-01/RDPD-2007) and the Director, CSIR-CGCRI, India and Director, CSIR-IICB for their generous and kind support to this work. We sincerely thank all the personnel who aided in the characterisation of the materials.

References

[1] H.B. El-Serag, Hepatocellular carcinoma, New England Journal of Medicine 365 (12) (2011) 1118–1127.
[2] K.A. McGlynn, L. Tsao, A.W. Hsing, S.S. Devesa, J.F. Fraumeni Jr., International trends and patterns of primary liver cancer, International Journal of Cancer 94 (2) (2001) 290–296.
[3] H.B. El-Serag, A.C. Mason, Rising incidence of hepatocellular carcinoma in the United States, New England Journal of Medicine 340 (10) (1999) 745–750.
[4] K. Ikeda, S. Saitoh, I. Koida, Y. Arase, A. Tsubota, K. Chayama, H. Kumada, M. Kawanishi, A multivariate analysis of risk factors for hepatocellular carcinogenesis: a prospective observation of 795 patients with viral and alcoholic cirrhosis, Hepatology 18 (1) (1993) 47–53.
[5] K.M. Mohandas, Hepatitis B associated hepatocellular carcinoma: epidemiology, diagnosis and treatment, Hepatitis B Annual 1 (1) (2004) 140–152.
[6] C.L. Lai, P.C. Wu, G.C. Chan, A.S. Lok, H.J. Lin, Doxorubicin versus no antitumor therapy in inoperable hepatocellular carcinoma. A prospective randomized trial, Cancer 62 (3) (1988) 479–483.
[7] J.M. Llovet, M.I. Real, X. Montana, R. Planas, S. Coll, J. Aponte, C. Ayuso, M. Sala, J. Muchart, R. Sola, J. Rodes, J. Bruix, Arterial embolisation or chemoembolisation versus symptomatic treatment in patients with unresectable hepatocellular carcinoma: a randomised controlled trial, Lancet 359 (9319) (2002) 1734–1739.
[8] R.G. Simonetti, A. Liberati, C. Angiolini, L. Pagliaro, Treatment of hepatocellular carcinoma: a systematic review of randomized controlled trials, Annals of Oncology 8 (2) (1997) 117–136.

[9] S.V. Ambudkar, S. Dey, C.A. Hrycyna, M. Ramachandra, I. Pastan, M. M. Gottesman, Biochemical, cellular, and pharmacological aspects of the multidrug transporter, Annual Review of Pharmacology and Toxicology 39 (1999) 361–398.
[10] R. Krishna, L.D. Mayer, Multidrug resistance (MDR) in cancer. Mechanisms, reversal using modulators of MDR and the role of MDR modulators in influencing the pharmacokinetics of anticancer drugs, European Journal of Pharmaceutical Sciences (2000) 265–283.
[11] B. Ringe, R. Pichlmayr, C. Wittekind, G. Tusch, Surgical treatment of hepatocellular carcinoma: experience with liver resection and transplantation in 198 patients, World Journal of Surgery 15 (2) (1991) 270–285.
[12] A. Chonn, P.R. Cullis, Recent advances in liposomal drug-delivery systems, Current Opinion in Biotechnology 6 (6) (1995) 698–708.
[13] R.L. Hong, Y.L. Tseng, F.H. Chang, Pegylated liposomal doxorubicin in treating a case of advanced hepatocellular carcinoma with severe hepatic dysfunction and pharmacokinetic study, Annals of Oncology 11 (3) (2000) 349–353.
[14] S.V. Dorozhkin, Bioceramics based on calcium orthophosphates, Glass and Ceramics 64 (11) (2007) 442–447 (Review).
[15] S.V. Dorozhkin, In vitro mineralization of silicon containing calcium phosphate bioceramics, Journal of the American Ceramic Society 90 (1) (2007) 244–249.
[16] S.K. Nandi, S. Roy, P. Mukherjee, B. Kundu, D.K. De, D. Basu, Orthopaedic applications of bone graft and graft substitutes: a review, Indian Journal of Medical Research 132 (7) (2010) 15–30.
[17] S.K. Nandi, P. Mukherjee, S. Roy, B. Kundu, D.K. De, D. Basu, Local antibiotic delivery systems for the treatment of osteomyelitis—A review, Materials Science and Engineering C–Materials for Biological Applications 29 (8) (2009) 2478–2485.
[18] B. Kundu, C. Soundrapandian, S.K. Nandi, P. Mukherjee, N. Dandapat, S. Roy, B.K. Datta, T.K. Mandal, D. Basu, R.N. Bhattacharya, Development of new localized drug delivery system based on ceftriaxone–sulbactam composite drug impregnated porous hydroxyapatite: a systematic approach for in vitro and in vivo animal trial, Pharmaceutical Research 27 (8) (2010) 1659–1676.
[19] B. Kundu, M.K. Sinha, M.K. Mitra, D. Basu, Fabrication and characterization of porous hydroxyapatite ocular implant followed by an in vivo study in dogs, Bulletin of Materials Science 27 (2) (2004) 133–140.
[20] M.P. Ferraz, A.Y. Mateus, J.C. Sousa, F.J. Monteiro, Nanohydroxyapatite microspheres as delivery system for antibiotics: release kinetics, antimicrobial activity, and interaction with osteoblasts, Journal of Biomedical Materials Research Part A 81 (4) (2007) 994–1004.
[21] N. Pramanik, A. Tarafdar, P. Pramanik, Capping agent-assisted synthesis of nanosized hydroxyapatite: comparative studies of their physicochemical properties, Journal of Materials Processing Technology 184 (1–3) (2007) 131–138.
[22] S. Yu, G.M. Chow, Carboxyl group (–CO_2H) functionalized ferrimagnetic iron oxide nanoparticles for potential bio-applications, Journal of Materials Chemistry 14 (18) (2004) 2781–2786.
[23] D.-G. Yu, J.H. An, J.Y. Bae, Y.E. Lee, S.D. Ahn, S.-Y. Kang, K.S. Suh, Preparation and characterization of titanium dioxide core/polymer shell hybrid composite particles prepared by emulsion polymerization, Journal of Applied Polymer Science 92 (5) (2004) 2970–2975.
[24] R. Chouhan, A. Bajpai, Real time in vitro studies of doxorubicin release from PHEMA nanoparticles, Journal of Nanobiotechnology 7 (2009) 5.
[25] W.J. Pigram, W. Fuller, L.D. Hamilton, Stereochemistry of intercalation: interaction of daunomycin with DNA, Nature New Biology 235 (53) (1972) 17–19.
[26] E. Tkalcec, M. Sauer, R. Nonninger, H. Schmidt, Sol–gel-derived hydroxyapatite powders and coatings, Journal of Materials Science 36 (21) (2001) 5253–5263.
[27] T.S.B. Narasaraju, D.E. Phebe, Some physico-chemical aspects of hydroxylapatite, Journal of Materials Science 31 (1) (1996) 1–21.
[28] Y. Suetsugu, I. Shimoya, J. Tanaka, Configuration of carbonate ions in apatite structure determined by polarized infrared spectroscopy, Journal of the American Ceramic Society 81 (3) (1998) 746–748.
[29] A.K. Bajpai, A. Mishra, Preparation and characterization of tetracycline-loaded interpenetrating polymer networks of carboxymethyl cellulose and poly(acrylic acid): water sorption and drug release study, Polymer International 54 (10) (2005) 1347–1356.
[30] S. Ganta, H. Devalapally, A. Shahiwala, M. Amiji, A review of stimuli-responsive nanocarriers for drug and gene delivery, Journal of Controlled Release 126 (3) (2008) 187–204.
[31] A. Ghosh, D. Ghosh, S. Sarkar, A.K. Mandal, S.T. Choudhury, N. Das, Anticarcinogenic activity of nanoencapsulated quercetin in combating diethylnitrosamine-induced hepatocarcinoma in rats, European Journal of Cancer Prevention 21 (1) (2012) 32–41.
[32] L.X. Qin, Z.Y. Tang, The prognostic molecular markers in hepatocellular carcinoma, World Journal Gastroenterology 8 (3) (2002) 385–392.